Talanta 134 (2015) 745–753

Contents lists available at ScienceDirect

Talanta

journal homepage: www.elsevier.com/locate/talanta

A new electrochemical sensor for the simultaneous determination of acetaminophen and codeine based on porous silicon/palladium nanostructure

Ali A. Ensafi*, Najmeh Ahmadi, Behzad Rezaei, Mehdi Mokhtari Abarghoui

Department of Chemistry, Isfahan University of Technology, Isfahan 84156-83111, Iran

ARTICLE INFO

Article history:
Received 27 October 2014
Received in revised form
18 December 2014
Accepted 19 December 2014
Available online 30 December 2014

Keywords:
Porous silicon/palladium nanostructure
Acetaminophen
Codeine
Differential pulse voltammetry
Simultaneous determination

ABSTRACT

A porous silicon/palladium nanostructure was prepared and used as a new electrode material for the simultaneous determination of acetaminophen (ACT) and codeine (COD). Palladium nanoparticles were assembled on porous silicon (PSi) microparticles by a simple redox reaction between the Pd precursor and PSi in an aqueous solution of hydrofluoric acid. This novel nanostructure was characterized by different spectroscopic and electrochemical techniques including scanning electron microscopy, X-ray diffraction, energy dispersive X-ray spectroscopy, fourier transform infrared spectroscopy and cyclic voltammetry. The high electrochemical activity, fast electron transfer rate, high surface area and good antifouling properties of this nanostructure enhanced the oxidation peak currents and reduced the peak potentials of ACT and COD at the surface of the proposed sensor. Simultaneous determination of ACT and COD was explored using differential pulse voltammetry. A linear range of 1.0–700.0 $\mu mol\ L^{-1}$ was achieved for ACT and COD with detection limits of 0.4 and 0.3 $\mu mol\ L^{-1}$, respectively. Finally, the proposed method was used for the determination of ACT and COD in blood serum, urine and pharmaceutical compounds.

1. Introduction

Acetaminophen (ACT, N-acetyl-p-aminophenol), commonly known as paracetamol, is commonly used as an antipyretic and analgesic medicine, which is considered safe at therapeutic levels for humans with normal drug use [1]. Overdoses of this drug lead to the accumulation of toxic metabolites, which may cause hepatoxicity and nephrotoxicity [2,3].

Codeine (COD), or methylmorphine, is an alkaloid belonging to the family of opiates naturally found in the poppy plant [4]. COD has long been used as an effective analgesic and antitussive agent in pharmaceutical preparations [5]. COD is rapidly adsorbed from the gastrointestinal tract to be subsequently distributed through intravascular spaces to various body tissues, with preferential uptake by parenchymatous organs such as the liver, spleen, and kidney.

In some drug formulations, ACT and COD are combined to provide adequate pain relief with reduced dose-dependent adverse effects. The combination provides effective pain relief by about 40% higher than that offered by the same dose of ACT alone [6]. The large scale therapeutic uses of ACT and COD require fast, simple and sensitive methods to be developed for their determination. Spectrophotometry, high-performance liquid chromatography, chemiluminescence, and electrochemical methods have been already used for their determination in pharmaceutical formulations and biological fluids [7–14], among which, electrochemical methods have attracted more attention for their high sensitivity, simplicity, reproducibility and low cost.

Recently, the unique properties of nanomaterials have made them attractive for a wide range of electrochemical sensing applications [15–18]. Compared to other nanomaterials, palladium nanoparticles have a high electrocatalytic activity towards some organic compounds due to their ability to adsorb and dissolve hydrogen [19]. Porous silicon (PSi) was first discovered accidentally by Uhlir [20] in 1956. Later, it became popular in different research areas in the early 1990s when Canham discovered its photoluminescence [21] and it has ever since found wide applications in bio-technology [22], drug delivery [23], energetic materials [24] and catalysis [25]. Moreover, a growing interest has been shown to PSi in sensor applications not only for its high surface area [26] and biocompatibility [27] but also because its pore size and morphology can be modulated by varying its synthesis conditions [28–31].

In this work, a new nanostructure is synthesized by galvanic loading of palladium nanoparticles on PSi via a simple redox reaction between Pd ions and PSi in an aqueous solution of HF. The nanocomposite combines the unique properties of porous silicon and the

* Corresponding author. Tel.: +98 311 3912351; fax: +98 311 3912350.
E-mail addresses: aaensafi@gmail.com, Ensafi@cc.iut.ac.ir (A.A. Ensafi).

http://dx.doi.org/10.1016/j.talanta.2014.12.028
0039-9140/

electrocatalytic activity of palladium nanoparticles. The novel nanostructure was then characterized by different spectroscopic and electrochemical techniques including field emission scanning electron microscopy (FE-SEM), X-ray diffraction (XRD), energy dispersive X-ray spectroscopy (EDX), fourier transform infrared spectroscopy (FT-IR) and cyclic voltammetry (CV). PSi surface shows interesting features for a wide variety of applications as they can be modified with readily available chemicals such as silanes under mild reaction conditions. Because PSi can act as both a reducing agent and a porous template, it was selected and was used as a substrate for the fast and facile synthesis of palladium nanoparticles without any reducing agent added. Moreover, palladium nanoparticles exhibit an improved chemical and electrochemical stability when loaded on the surface of PSi as a support, which leads to the high stability of the PSi/Pd nanostructure based sensor thus developed.

The enhanced oxidation peaks current and reduced peaks potential of ACT and COD at the surface of the modified electrode are the results of the high electrochemical activity, fast electron transfer rate, high surface area and good antifouling properties of this nanostructure. Hydrodynamic amperometry and differential pulse voltammetry (DPV) were used for the determination of these species to find that the newly developed electrode exhibits a good performance toward the simultaneous determination of ACT and COD. Moreover, its simplicity and reliability with a wide linear dynamic range, low detection limit and good selectivity made this sensing platform useful for the routine analysis of ACT and COD in clinical and pharmaceutical applications. Table 1 shows a list of the different electrochemical sensors used for the individual or simultaneous determination of ACT and COD [14,19,32–38]. Based on the detection limits and linear response ranges recorded, the sensor proposed in this work not only compares well with but also outperforms the other sensors listed in the table.

2. Experimental

2.1. Chemicals and apparatus

Acetaminophen and codeine phosphate were purchased from Temad Co, Iran. Polycrystalline Si powder (325 meshes, 99%) and multiwall carbon nanotubes (MWCNTs) were purchased from Sigma-Aldrich. All other chemicals such as sodium hydroxide, nitric acid, hydrofluoric acid, palladium sulfate, graphite and paraffin oil were of analytical grade and purchased from Merck. All solutions were prepared with deionized water.

Britton–Robinson universal buffer was prepared by dissolving 5.0 g of boric acid, 2.7 mL of concentrated phosphoric acid (85% w/w) and 2.3 mL glacial acetic acid in water and diluting to 1.0 L with water. The pH of the buffer was adjusted using 0.1 mol L^{-1} NaOH solution.

Electrochemical measurements were performed by a computer controlled Autolab (PGSTAT302N, Eco-Chemie, The Netherlands) with GPES-4.9 software. A conventional three-electrode cell was used with the modified working electrode, a saturated Ag/AgCl reference electrode and a platinum wire auxiliary electrode. A Metrohm 827 pH-meter with a glass electrode was used for pH adjustments.

DPV measurements of ACT or COD or their mixtures were performed in 0.1 mol L^{-1} Britton–Robinson buffers with different pH. A FE-SEM (Hitachi S4160) at an accelerating voltage of 20 kV was used for examination of the nanocomposites morphology. The XRD patterns of the as synthesized material was measured using a Bruker D_8/Advance X-ray diffractometer with Cu-K_α radiation from 20° to 100°. The EDX spectra of the synthesized material was recorded using a Philips XLS instrument in ambient conditions.

FT-IR spectra was recorded using a JASCO FT-IR (680 plus) spectrometer, using pellets of the nanostructures (diluted with KBr).

2.2. Synthesis of the porous silicon/palladium nanostructure

PSi powder was prepared using the chemical etching method described in our previous work [39]. Briefly, about 1.0 g of Si-powder (325 mesh) was dispersed in 100 mL of the etching solution that consisted of HF, HNO_3, and H_2O with molar ratios of 4.0, 1.0 and 30.0, respectively. After 10 min of mild stirring, the initial metallic color of the silicon powder converted to a brown-yellow one, indicating the formation of PSi. The partial surface oxidation of Si particles, which leads to the conversion of Si into PSi, can be expressed by the following reaction:

$$3Si + 4HNO_3 + 18HF \rightarrow 3H_2SiF_6 + 4NO + 8H_2O \qquad (Si \rightarrow PSi) \qquad (1)$$

During the etching process, the fluoride ions attack Si atoms at the Si–electrolyte interface to produce a fluorinated surface, which immediately dissolves to form SiF_6^{-2} and leaves behind holes on the surface of the PSi particles.

The resulting mixture was then washed with distilled water several times before being dried at room temperature for 8 h to obtain the PSi powder.

The porous silicon/palladium nanostructure (PSi/Pd-NS) was prepared via a simple redox reaction between Pd ions and PSi in an aqueous solution of hydrofluoric acid (HF) without any reducing agents used. For this purpose, about 0.25 g of the PSi powder

Table 1
Comparison of different electrochemical sensors with the proposed sensor for determination of ACT and COD.

Working electrode	ACT		COD		Technique	Reference
	Linear range (μmol L^{-1})	Detection limit (μmol L^{-1})	Linear range (μmol L^{-1})	Detection limit (μmol L^{-1})		
BDDF	–	–	0.1–60	0.08	DPV	[14]
PdPAlE	290–3300	–	3000–40000	NR	CV	[19]
SWCNT/GNS	0.05–64.5	0.038	–	–	DPV	[32]
PEDOT/GO	10.0–60	0.57	–	–	CV	[33]
Pd/GO	0.005–80	0.002	–	–	DPV	[34]
SWCNT/CCE	–	–	0.2–230	0.11	DPV	[35]
GRBME	–	–	0.05–30	0.015	SWV	[36]
AlEMPd	100–3000	5	100–3000	5	DPV	[37]
GR/$CoFe_2O_4$	0.03–12	0.025	0.03–12	0.011	SWV	[38]
PSi/Pd–NS/CNTPE	1–700.0	0.4	1–700.0	0.3	DPV	This work
PSi/Pd-NS/CNTPE	0.4–353.5	0.1	0.5–557.5	0.2	Amperometry	This work

BDDF: boron-doped diamond film; PdPAlE: palladium-plated aluminum electrode; SWCNT/GNS: single-walled carbon nanotube–graphene nanosheet; PEDOT/GO: poly(3,4-ethylenedioxythiophene)/graphene oxide; Pd/GO: Pd/graphene oxide; SWV:square wave voltammetry. SWCNT/CCE: single-walled carbon nanotube/carbon ceramic electrodeclay; GRBME: graphene based modified electrode; AlEMPd: aluminum electrode modified by thin layer of palladium; GR/$CoFe_2O_4$: graphene/$CoFe_2O_4$.

was dispersed in 100 mL of 0.10 mol L^{-1} HF solution. Then, 5 mL of 0.050 mol L^{-1} palladium sulfate was added dropwise by vigorous stirring for 10 min so that it would spread well on the surface of PSi. The corresponding half reactions involved in the galvanic loading of Pd nanoparticles on PSi surface are as follows:

$$Si + 6F^- \rightarrow SiF_6^{2-} + 4e^- \qquad (SiF_6^{2-} + 4e^- \rightarrow Si + 6F^- E^0/V = -1.240) \quad (2)$$

$$Pd^{2+} + 2e^- \rightarrow Pd \qquad E^0/V = +0.951 \quad (3)$$

The resulting PSi/Pd-NS was filtered and washed with plenty of water before being dried in atmosphere.

2.3. Electrochemical sensor preparation

A bare carbon paste electrode (CPE) was fabricated by hand mixing of graphite powder and paraffin oil at a ratio of 70/30 (w/w). Carbon nanotube paste electrode (CNTPE) was fabricated by mixing 30 mg of paraffin oil, 60 mg of graphite powder and 10 mg of MWCNTs. PSi/Pd-NS/CNTPE was fabricated by mixing 30 mg of paraffin oil, 56 mg of graphite powder, 10 mg of MWCNTs and 4 mg of the PSi/Pd-NS. The mixture was then mixed well in an agate mortar for 20 min until a uniformly wetted paste was obtained. The resulting paste was inserted into the end of a polyethylene syringe (i.d.: 2.0 mm). An electrical connection was made using a stainless steel stick. When necessary, a new surface was obtained by pushing an excess of the paste out of the syringe followed by polishing it on a weighing paper.

2.4. General procedure and real sample preparation

The modified electrode was polished on a weighing paper. The blank (I_b) and analytical (I_a) signals, in 0.1 mol L^{-1} of Britton–Robinson buffer (pH 5.0), were recorded in the potential range of 0.00 to +1.30 V vs. Ag/AgCl using DPV with a pulse amplitude of 0.06 V, a pulse width of 0.04 s and a pulse period of 0.5 s.

Three different brands of Acetaminophen–Codeine® tablets labeled as containing 300 mg of ACT and 10 mg of COD per tablet were bought from a local pharmacy. Five tablets of each brand were ground and homogenized to a fine powder. Then, 4.0 mg of each was accurately weighed and dissolved in 100 mL of Britton–Robinson buffer (0.1 mol L^{-1}, pH 5.0) by ultrasonication for 10 min. Finally, the resulting solution was filtered through a 0.45 μm filter and analyzed for its ACT and COD contents by the proposed method.

Urine and blood plasma samples were centrifuged (2500 rpm) for 5 min. The supernatant was filtered using a 0.45 μm pore size filter and diluted 10 times with a 0.1 mol L^{-1} of Britton–Robinson buffer at pH 5.0. The standard addition method was used for the determination of ACT and COD contents in real samples.

3. Results and discussion

3.1. Characterization of the porous silicon/palladium nanostructure

The SEM micrograph of PSi/Pd-NS (Fig. 1A) shows that Pd nanoparticles with an average diameter of about 80 nm were uniformly distributed on the surface of PSi. Fig. 1B shows the XRD pattern

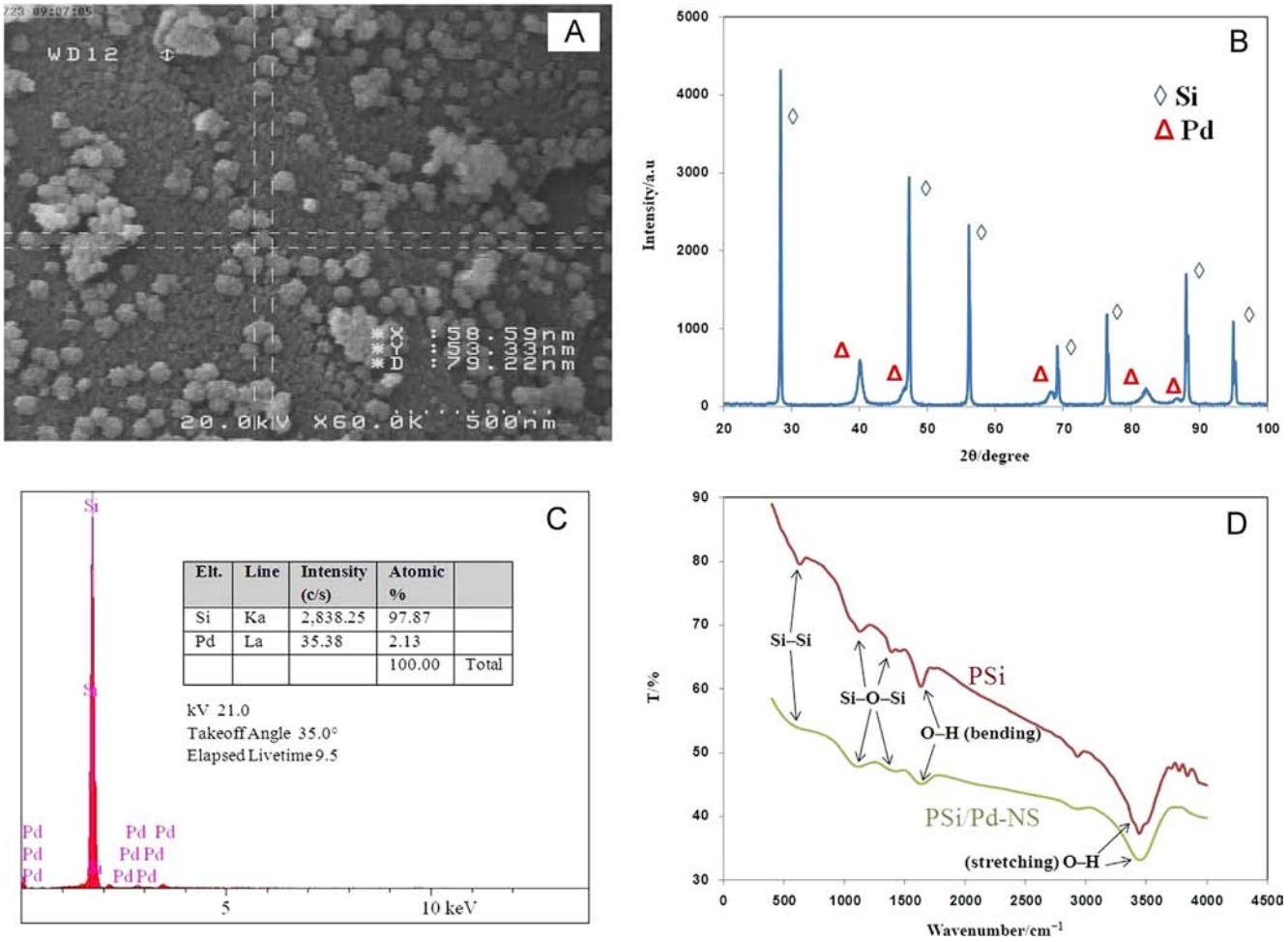

Fig. 1. SEM micrograph (A); XRD pattern (B); and EDX spectra (C) of PSi/Pd nanostructure. (D): FT-IR spectra of PSi and PSi/Pd nanostructure.

of the PSi/Pd-NS. The strong diffraction peaks at Bragg angles of 28.6°, 47.3°, 56.5°, 69.6°, 76.2°, 88.0° and 95.1° can be assigned to Si (111), Si (220), Si (311), Si (400), Si (331), Si (422) and Si (333), respectively [40]. The peaks around $2\theta = 39.8°$, 47.0°, 67.7°, 83.4° and 87.6° can be attributed to the diffraction peaks of Pd crystal faces (111), (200), (220), (311) and (222), respectively indicating Pd nanoparticles in a face-centered cubic (fcc) structure [41]. The results of the bulk composition analysis obtained from EDX (Fig. 1C) revealed that the nanostructure contained 79.87 mol% Si and 2.13 mol% Pd, indicating that the PSi/Pd-NS was successfully synthesized.

Before galvanic loading of Pd nanoparticles, FT-IR spectra of PSi were recorded and compared with those obtained for PSi/Pd-NS (Fig. 1D). The results showed that the presence of Pd nanoparticles on the surface of PSi caused no major changes in the nature of either the vibration modes or the bonds present in the PSi, except that the overall intensity was reduced and the intensities of the major peaks were changed only slightly. Representative PSi peaks (Si–Si stretching modes at 620 cm^{-1}, Si–O–Si stretching modes at 1000 to 1300 cm^{-1}, O–H bending vibration modes at 1630 cm^{-1} and O–H stretching vibrations at 3450 cm^{-1}) were observed in the FT-IR spectra of both PSi and PSi/Pd-NS [39].

To investigate the electrochemical behavior of the PSi/Pd-NS modified electrode, 0.5 mol L^{-1} of H_2SO_4 solution was selected as a suitable electrolyte. The peaks of the modified electrode observed in the cyclic voltammograms can be assigned to the hydrogen

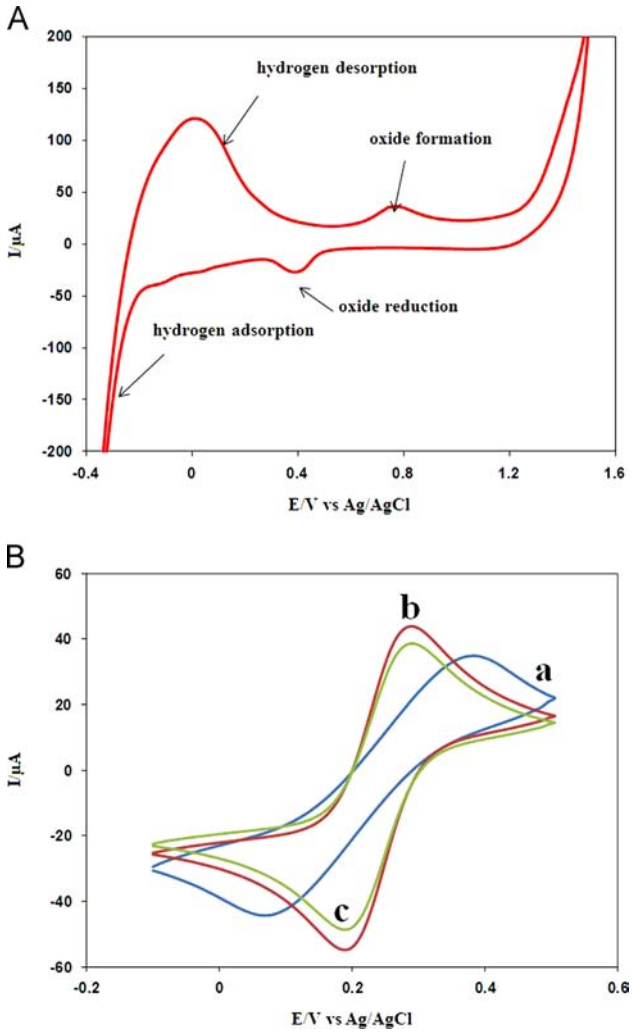

Fig. 2. A: Cyclic voltammogram of PSi/Pd-NS/CNTPE in 0.5 mol L^{-1} H_2SO_4. B: Cyclic voltammograms of unmodified CPE (a), CNTPE (b) and PSi/Pd-NS/CNTPE (c), in 0.5 mmol L^{-1} $K_3[Fe(CN)_6]$ in the presence of 0.1 mol L^{-1} KNO_3.

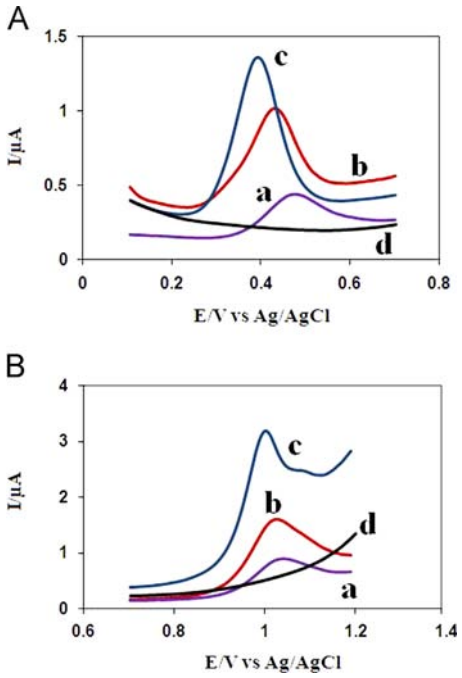

Fig. 3. DPV of 20.0 μmol L^{-1} of ACT (A) and COD (B) at unmodified CPE (curve a), CNTPE (curve b) and PSi/Pd-NS/CNTPE (curve c) at pH 5.0 with accumulation time of 150 s. Curve d is DPV of PSi/Pd-NS/CNTPE in the absence of ACT (A) and COD (B).

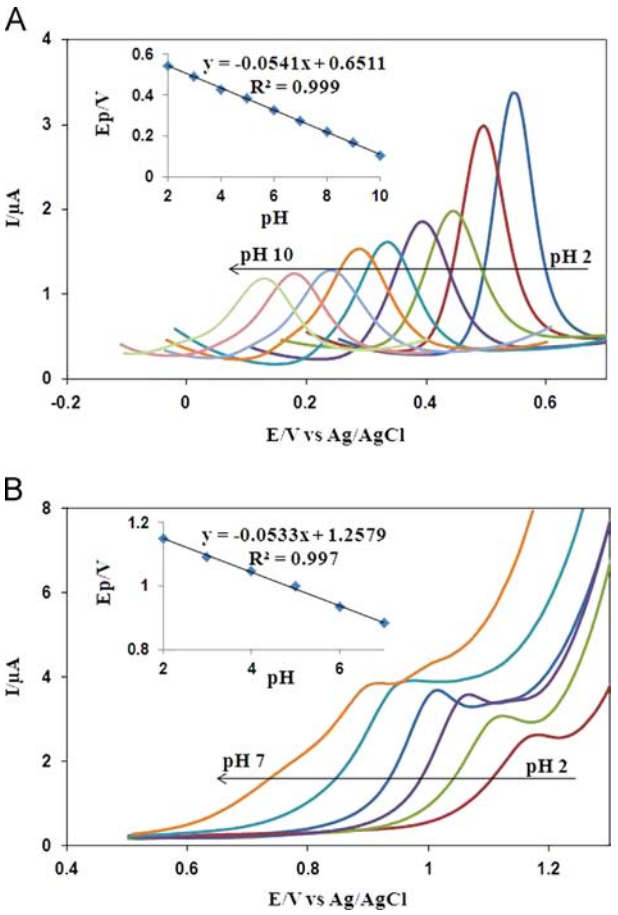

Fig. 4. Effect of pH on the electrochemical oxidation of 30.0 μmol L^{-1} ACT (A) and COD (B) at the surface of PSi/Pd-NS/CNTPE with accumulation time 150 s. Insets: Plot of the oxidation peaks potential vs. the solution pH.

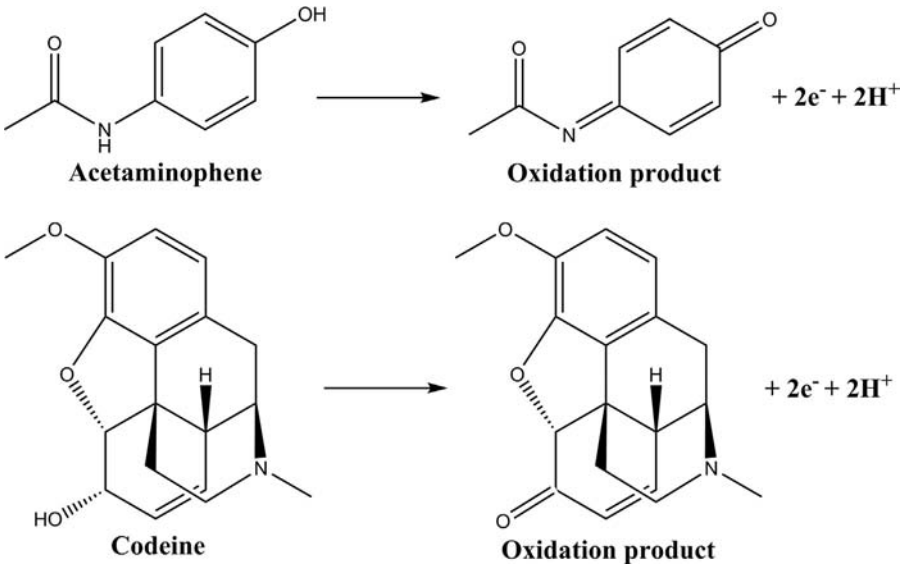

Scheme 1. Electrooxidation mechanism of ACT and COD at PSi/Pd-NS/CNTPE.

adsorption/desorption and Pd oxidation/reduction (Fig. 2A). The two peaks at 750 and 400 mV may be attributed to the surface hydroxide/oxide formation ($Pd(OH)_2$/PdO) and the surface oxide/hydroxide reduction, respectively [42]. The other two peaks correspond to the adsorption and desorption of hydrogen atoms during the cathodic and anodic sweeps [42].

For further characterization, the cyclic voltammetric behavior of the $Fe(CN)_6^{3-}$ (as a probe) at the surfaces of CPE, CNTPE and PSi/Pd-NS/CNTPE were studied (Fig. 2B). The CPE showed a couple of redox peaks with a peak-to-peak separation (ΔE_p) of 300 mV (curve a). At the surface of CNTPE, the redox peak currents of the probe increased significantly compared to those observed for CPE whereas the peak-to-peak separation (ΔE_p) decreased to 80 mV, indicating that MWCNTs effectively enhanced the electron transfer rate due to their upstanding electrical conductivity (curve b). For the PSi/Pd-NS/CNTPE, incorporation of PSi/Pd-NS and MWCNTs in the CPE significantly increased the redox peak currents compared to the case of unmodified CPE, whereas a slight decrease was observed in the redox peak current compared to the case of CNTPE due to the semiconductive properties of the PSi (curve c).

3.2. Electrochemical oxidation of ACT and COD on the surface of the PSi/Pd-NS/CNTPE

Direct electrochemical oxidation of ACT and COD on the surfaces of CPE, CNTPE and PSi/Pd-NS/CNTPE were studied using the DVP technique at pH 5.0 (Fig. 3). The oxidation signals of ACT and COD on the surface of the PSi/Pd-NS/CNTPE exhibited significant enhancements in the peaks current and lower overpotentials compared to those obtained for unmodified CPE or CNTPE. The above results may explain the specific and superior properties of Pd nanoparticles and PSi, such as their high surface area, good antifouling property and high electrocatalytic activity toward the oxidation of ACT and COD.

The effect of accumulation time on the oxidation peaks current of ACT and COD on the surface of the PSi/Pd-NS/CNTPE was also investigated at pH 5.0 under open circuit conditions. The results (data not shown) revealed that the oxidation peaks current of both ACT and COD increased with increasing accumulation time. However, after 120 s, the oxidation signal of ACT remained unchanged whereas that of COD reached a constant value after 150 s, which indicates the saturation of the electrode surface. Therefore, 150 s was chosen as the optimum accumulation time in subsequent experiments.

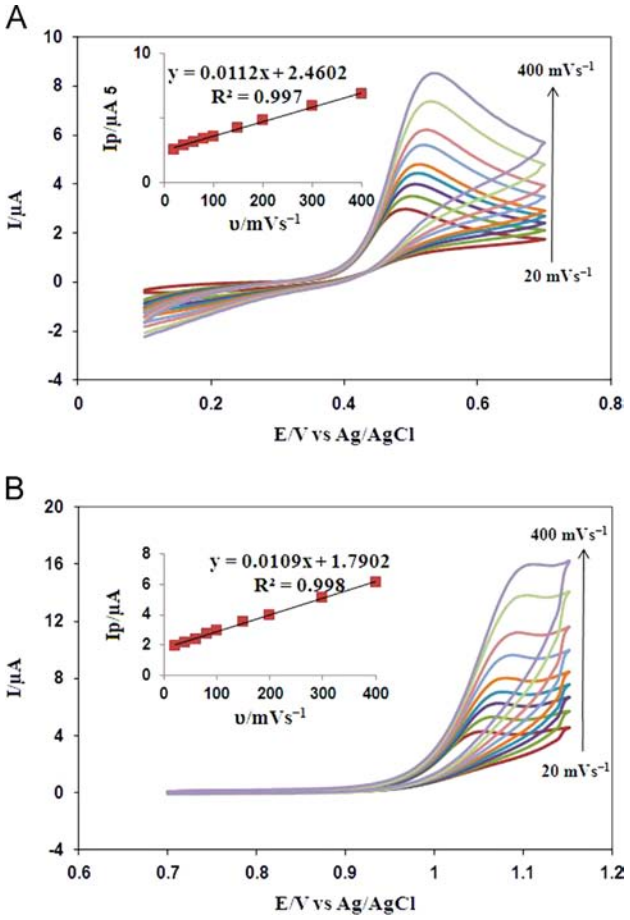

Fig. 5. Effect of different scan rates on cyclic voltammograms of 200.0 μmol L^{-1} of (A): ACT and (B): COD, at the surface of PSi/Pd-NS/CNTPE at pH 5.0 with accumulation time of 150 s. Insets: plot of the oxidation peaks current vs. the scan rate.

The effect of accumulation potential on the peaks current was also investigated in potential ranges of 0–300 mV and 0–900 mV for ACT and COD, respectively. No significant effects were observed on the peaks current as a result of variation in the accumulation potential such that the signals were almost identical to those observed for the

open circuit conditions (data not shown). This is due to the fact that, at pH 5.0, neither of the analytes has any negative charge for being electrostatically attracted to the electrode surface. Therefore, the subsequent experiments were carried out under the open-circuit conditions.

The effect of sample solution pH on the electrochemical responses of ACT and COD on the surface of the PSi/Pd-NS/CNTPE was also studied in the pH range of 2.0–10.0 for ACT and 2.0–7.0 for COD, using DPV in the Britton–Robinson buffer (Fig. 4A and B). Negative shifts were observed in the oxidation peaks of ACT and COD with increasing pH, indicating that protons took part in the electrochemical oxidation of these two species. pH dependence of the oxidation peaks potential were found to follow equations characterized by slopes of 54 and 53 mV per decade for ACT and COD, respectively (insets of Fig. 4). These slopes are close to the expected Nernstian theoretical value of 59.1 mV, suggesting that equal numbers of electrons and protons had been uptaken [13,36]. The ACT and COD oxidation mechanisms at the PSi/Pd-NS/CNTPE is shown in Scheme 1. Fig. 4 shows that the peak currents of COD increased with increasing the solution pH from 2.0 to 5.0, beyond which they decreased, whereas those of ACT decreased with increasing the solution pH. Therefore, pH 5.0 was chosen to achieve the required sensitivity to both ACT and COD in the following experiments.

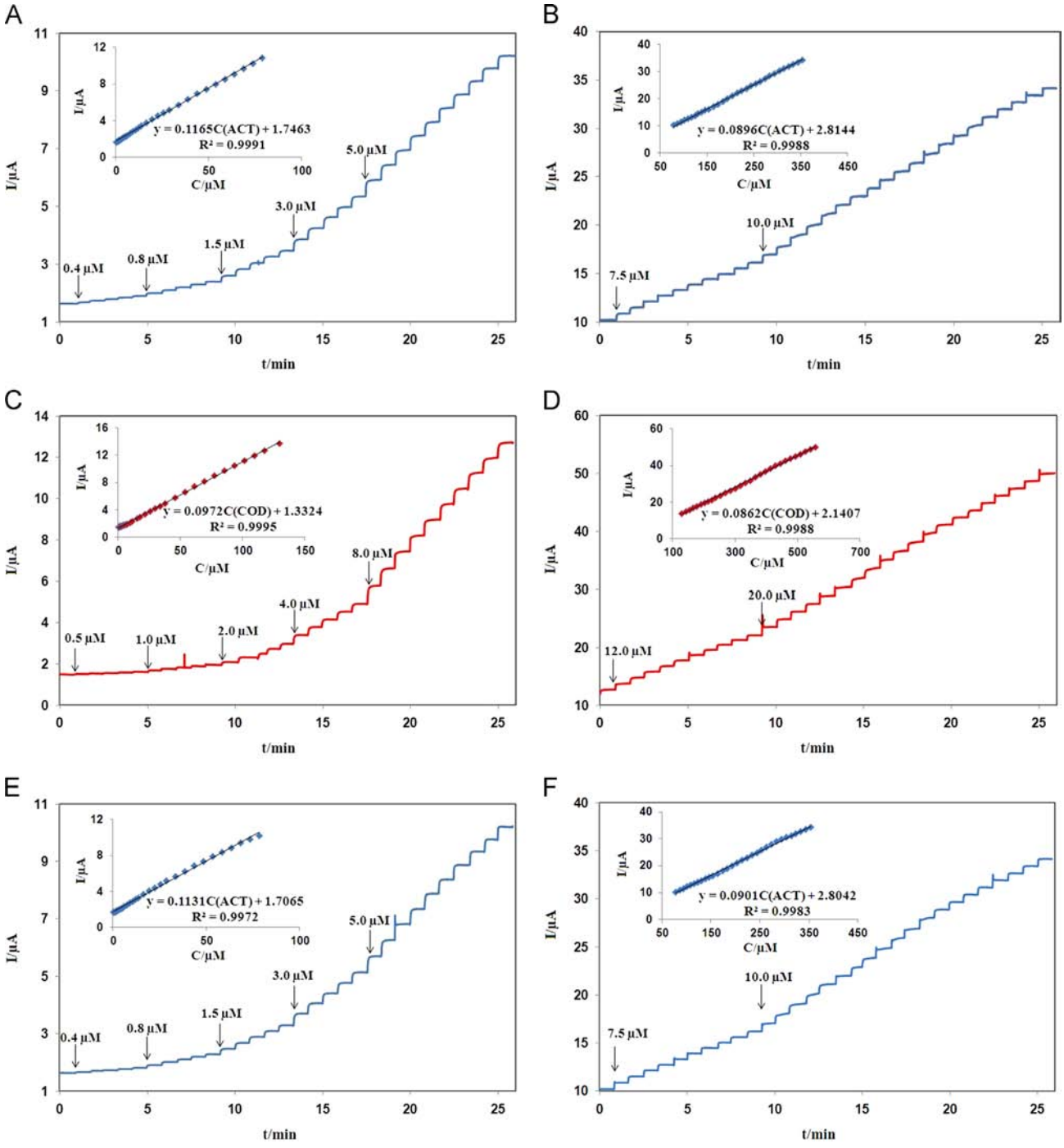

Fig. 6. Hydrodynamic amperograms of ACT (A and B), COD (C and D) and ACT in the presence of 100.0 µmol L^{-1} COD (E and F) at the surface of PSi/Pd-NS/CNTPE at pH 5.0. Insets: plot of the peaks current vs. the concentration.

Cyclic voltammograms of ACT and COD on the surface of the PSi/Pd-NS/CNTPE were also investigated at various scan rates. The results revealed that ACT and COD exhibit totally irreversible oxidations at the surface of the modified-electrode. As shown in Fig. 5, the relevant oxidation peaks current were proportional to the scan rates applied in the range of 20–400 mV s^{-1}, following the linear regression equations of $I_{pa}=0.0112\upsilon+2.4602$ ($R^2=0.997$) for ACT (Fig. 5A) and $I_{pa}=0.0109\upsilon+1.7902$ ($R^2=0.998$) for COD (Fig. 5B). These results indicate that these two electrochemical processes are surface controlled.

3.3. Amperometric determination of ACT and COD

Although the amperometric technique cannot be employed for the simultaneous determination of electroactive compounds, this method is an attractive option for the individual determination of these compounds. A major advantage of amperometric sensors vs. voltammetric sensors is their easy automation. Moreover, amperometric sensors provide a more stable and reproducible response, compared to their voltammetric counterparts. Both ACT and COD exhibit higher oxidation currents and lower overpotentials at the surface of the PSi/Pd-NS/CNTPE than at the surface of either CPE or CNTPE (Fig. 3). The differences may be ascribed to the high electrochemical activity and antifouling properties of the PSi/Pd nanostructure Thus, the sensor proposed in this study was used for the individual determinations of these two species using amperometric technique with a home-made rotating electrode and with applied potentials of 0.55 and 1.10 V vs. Ag/AgCl, respectively at pH 5.0.

Fig. 6A and B shows the amperometric curves of the rotating (2000 rpm) PSi/Pd-NS/CNTPE with successive additions of ACT and Fig. 6C and D shows the curves for COD at the same electrode. A linear dependence is observed between the current and ACT concentration in the range of 0.4–353.5 μmol L^{-1} with a detection limit of 0.10 μmol L^{-1} (signal-to-noise ratio of 3); for COD, however, the dependence between the current and COD concentration is clearly linear in the range of 0.5–557.5 μmol L^{-1} with a detection limit of 0.20 μmol L^{-1} (insets of Fig. 6 present the calibration curves of ACT and COD).

Amperometric determination of ACT in the presence of COD was also employed to examine the intermolecular effects of these two analytes. For this purpose, the amperometric curve of ACT in the presence of a constant amount of COD (100 μmol L^{-1}) was recorded and compared with that obtained in the absence of COD (Fig. 6E and F). The results showed that the calibration equations for ACT (insets of Fig. 6) did not lead to any significant change in the absence or presence of COD. The proposed electrochemical sensor can, therefore, be used for the individual determination of ACT in the presence of COD using the hydrodynamic amperometric technique.

3.4. Simultaneous determination of ACT and COD

From a clinical point of view, simultaneous determination of ACT and COD is of great importance since these two drugs coexist in acetaminophen/codeine tablets. In order to determine whether the presence of ACT or COD interferes with the electrochemical determination of the other, the concentration of one species was varied with a constant concentration of the other. The DPVs of different concentrations of ACT or COD at a fixed concentration (200.0 μmol L^{-1}) of the other species were recorded (Fig. 7A and B). The results showed that the peak current of ACT increased when its concentration was increased, while the peak current of COD remained almost constant (Fig. 7A). Also, as shown in Fig. 7B, the peak current of ACT remained constant whereas that of COD increased when its concentration was

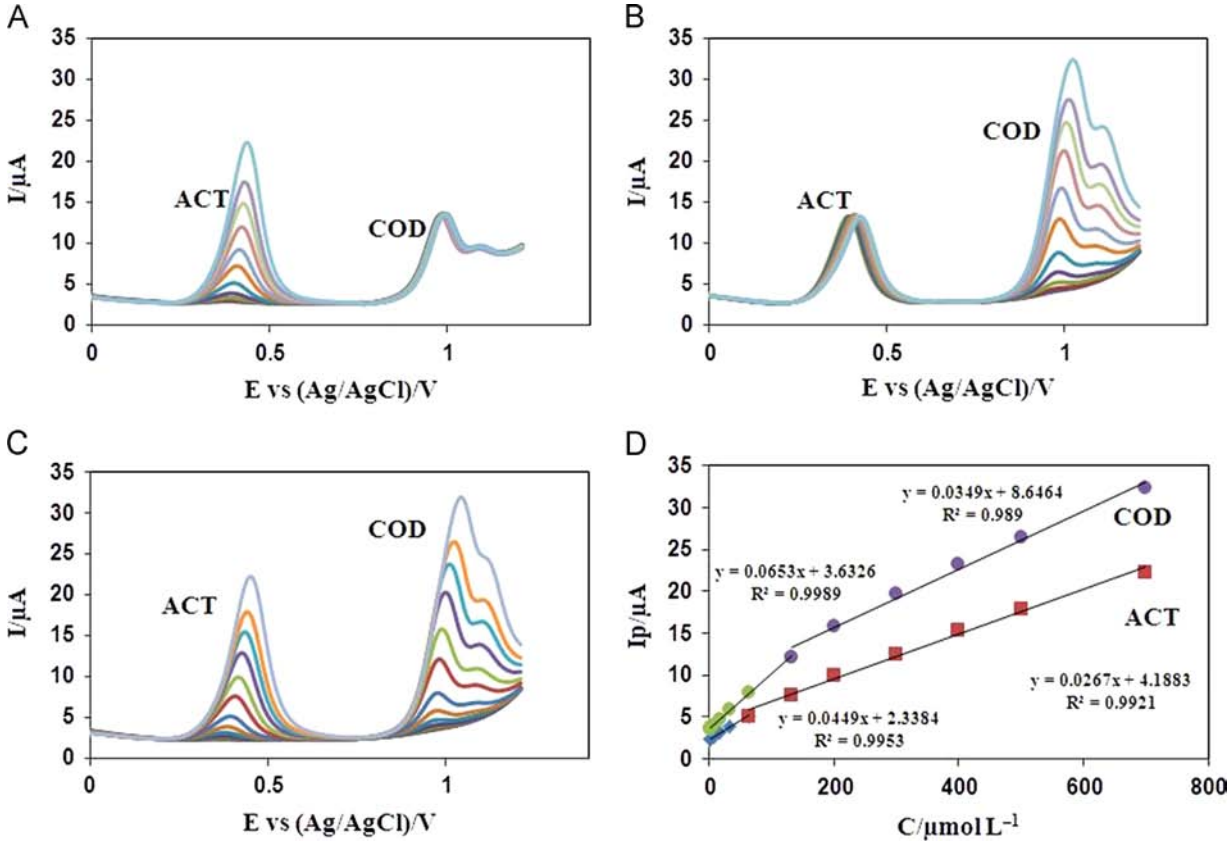

Fig. 7. DPVs of (A): Different concentrations of ACT (1.0–700.0 μmol L^{-1}) in the presence of 200.0 μmol L^{-1} COD; (B): Different concentrations of COD (1.0–700.0 μmol L^{-1}) in the presence of 200.0 μmol L^{-1} ACT solution; and (C): Simultaneous determination of ACT and COD (1.0–700.0 μmol L^{-1}); (D): Plots of I_p vs. ACT and COD concentrations in the simultaneous determination (accumulation time, 150 s; pH, 5.0).

Table 2
Simultaneous determination of ACT and COD in pharmaceutical tablets with our proposed sensor ($n=3$).

Sample number	ACT				COD			
	Labeled value/mg	Detected/mg	Recovery%	RSD%	Labeled value/mg	Detected/mg	Recovery%	RSD%
1	300	315	105	6	10	10.4	104	5
2	300	309	103	5	10	10.5	105	5
3	300	294	98	6	10	9.7	97	6

Table 3
Simultaneous determination of ACT and COD in urine and plasma samples using our proposed sensor ($n=3$).

Sample	Analyte	Added (μmol L^{-1})	Found (μmol L^{-1})	Recovery (%)
Urine	ACT	–	< Limit of detection	–
		7.50	7.82 ± 0.35	104.3
		15.00	15.42 ± 0.45	102.8
	COD	–	< Limit of detection	–
		7.50	7.80 ± 0.40	104.0
		15.00	14.37 ± 0.70	95.8
Blood Serum	ACT	–	< Limit of detection	–
		7.50	7.30 ± 0.25	97.3
		15.00	15.27 ± 0.35	101.8
	COD	–	< Limit of detection	–
		7.50	7.40 ± 0.25	98.6
		15.00	14.57 ± 0.45	97.1

increased. This means that the electrochemical signals of ACT and COD do not interfere with each other. These results confirm that the two species can be simultaneously determined by the proposed method.

Fig. 7C presents the voltammograms of ACT and COD when the concentrations of both compounds are simultaneously increased at the surface of the PSi/Pd-NS/CNTPE. Plots of the oxidation currents of ACT and COD vs. their concentrations (Fig. 7D) show two linear ranges for ACT (1.0–64.0 μmol L^{-1} and 64.0–700.0 μmol L^{-1}) and two linear ranges for COD (1.0–132.0 μmol L^{-1} and 132.0–700.0 μmol L^{-1}) with detection limits of 0.4 and 0.3 μmol L^{-1} (signal to noise ratio of 3) for ACT and COD, respectively.

3.5. Reproducibility and stability of the proposed sensor

The electrochemical responses of 30.0 μmol L^{-1} of ACT and COD were determined at five modified electrodes freshly prepared in order to determine the reproducibility of the proposed sensor. The RSD% values obtained for ACT and COD were 4.3% and 4.9%, respectively, indicating the reliability of the proposed sensor. Surface reproducibility of the PSi/Pd-NS/CNTPE was also investigated by six replicate measurements of ACT and COD. The RSD% values for the oxidation peaks current of 30.0 μmol L^{-1} of ACT and COD were 2.3% and 2.6%, respectively. The excellent reproducibility of the PSi/Pd-NS/CNTPE confirms that the electrode is not poisoned by the oxidation products of either ACT or COD and that it is capable of being used repeatedly. Moreover, the stability of the PSi/Pd-NS/CNTPE was examined by storing the electrode in the laboratory for 30 days. The eligible decrease in the electrode's response (less than 5%) indicated its satisfactory stability.

3.6. Effects of potential interfering species and analytical application of the electrode

The effects of potentially interfering species on the electrode selectivity were investigated using 2.0 μmol L^{-1} ACT and COD, under the optimum conditions. Tolerance limit was defined as the maximum concentration of the potentially interfering substance that led to an error of less than $\pm 6.0\%$. The results showed that 1000-fold concentration of Mg^{2+}, Fe^{3+}, Cl^-, SO_4^{2-}, HCO_3^- and NH_4^+; 500-fold concentration of cysteine, lactose, glucose, sucrose and tartaric acid; and 200-fold concentration of uric acid and ascorbic acid did not affect the oxidation peaks current of ACT or COD. These results confirmed that the proposed electrochemical sensor is free from interference by most potentially interfering substances in practical conditions.

As a real sample application, the PSi/Pd-NS/CNTPE was used to determine ACT and COD in pharmaceutical tablets, urine and blood plasma. For this purpose, the samples were prepared as described in the section on real sample preparation above and analyzed using the standard addition method. According to the data in Tables 2 and 3, the good accuracy (recovery) and precision (R.S.D) obtained demonstrate the reliability of the proposed sensor for the determination of ACT and COD in real samples.

4. Conclusion

In summary, a porous silicon/palladium nanostructure was prepared and characterized by different techniques of FE-SEM, XRD, EDX, FT-IR, and CV. The novel nanostructure was used as an electrocatalyst for the individual and simultaneous determinations of acetaminophen and codeine using hydrodynamic amperometry and DPV technique. Although some of electrochemical methods reported in the literature [32,34–36] might exhibit better sensitivity for the determination of ACT [32,34] or COD [35,36], they are not capable of measuring these analytes simultaneously. The combined antifouling properties of porous silicon and the electrocatalytic activity of palladium nanoparticles provide a new sensing surface for ACT and COD with long-term stability, good reproducibility, wide linear ranges and low detection limits. Finally, satisfactory results were obtained when the proposed sensor was applied for the determination of ACT and COD in clinical and pharmaceutical samples.

Acknowledgments

The authors express their appreciation to the Isfahan University of Technology (Iran) Research Councils and Center of Excellence in Sensor for financial support of this work.

References

[1] J.G.M. Bessems, N.P.E. Vermeulen, Crit. Rev. Toxicol. 31 (2001) 55–138.
[2] M.T. Olaleye, B.T.J. Roch, Exp. Toxicol. Pathol. 59 (2008) 319–327.
[3] M. Mazer, J. Perrone, J. Med. Toxicol. 4 (2008) 2–6.
[4] C.F. Thorn, T.E. Klein, R.B. Altman, Pharmacogenet. Genomic 19 (2009) 556–558.
[5] B.L. Velázquez, P. Lorenzo, A. Moreno, I. Lizasoain, J.C. Leza, M.A. Moro, A. Portolés, Farmacologia Basicay Clinica, 18th ed., Medica Panamericana, Madrid, 2008.
[6] L. Toms, S. Derry, R.A. Moore, H.J. McQuay, Cochrane Database Syst. Rev. 1 (2009) 1–88.
[7] J.T. Afshari, T.Z. Liu, Anal. Chim. Acta 443 (2001) 165–169.
[8] M.H. Mashhadizadeh, L. Jafari, J. Iran. Chem. Soc. 7 (2010) 678–684.
[9] J.C. Roberts, H.L. Phaneuf, J.G. Szakacs, R.T. Zera, J.G. Lamb, M.R. Franklin, Chem. Res. Toxicol. 11 (1998) 1274–1282.

[10] A. Manassra, M. Khamis, M. el-Dakiky, Z. Abdel-Qader, F. Al-Rimawi, J. Pharm. Biomed. Anal. 51 (2010) 991–993.
[11] W. Ruengsitagoon, S. Liawruangrath, A. Townshend, Talanta 69 (2006) 976–983.
[12] B. Rezaei, T. Khayamian, A. Mokhtari, J. Pharm. Biomed. Anal. 49 (2009) 234–239.
[13] C.X. Xu, K. Huang, Y. Fan, Z. Wu, J. Li, J. Mol. Liq. 165 (2012) 32–37.
[14] L. Svorc, J. Sochr, J. Svitkova, M. Rievaj, D. Bustin, Electrochim. Acta 87 (2013) 503–510.
[15] W.Z. Le, Y.Q. Liu, Sens. Actuators B 141 (2009) 147–153.
[16] X.M. Miao, R. Yuan, Y.Q. Chai, Y.T. Shi, Y.Y. Yuan, J. Electroanal. Chem. 612 (2008) 157–163.
[17] J.H. Shim, A Cha, Y. Lee, C. Lee, Electroanalysis 23 (2011) 2057–2062.
[18] P.R. Martins, M.A. Rocha, L. Angnes, H.E. Toma, K. Araki, Electroanalysis 23 (2011) 2541–2548.
[19] M.H. Pournaghi-Azar, S. Kheradmandi, A. Saadatirad, J. Solid State Electrochem. 14 (2010) 1689–1695.
[20] Auhlir, Bell Syst. Tech. J. 35 (1956) 333–347.
[21] L.T. Canham, Appl. Phys. Lett. 57 (1990) 1046–1048.
[22] M.J. Sweetman, J. Shearer, J.G. Shapter, N.H. Voelcker, Langmuir 27 (2011) 9497–9503.
[23] N.H. Maniya, S.R. Patel, Z.V.P. Murthy, Superlattice Microstruct. 55 (2013) 144–150.
[24] B.M. Bang, H. Kim, H.K. Song, J. Cho, S. Park, Energy Environ. Sci. 4 (2011) 5013–5019.
[25] S. Polisski, B. Goller, K. Wilson, D. Kovalev, V. Zaikowskii, A. Lapkin, J. Catal. 271 (2010) 59–66.
[26] A. Loni, D. Barwick, L. Batchelor, J. Tunbridge, Y. Han, Z.Y. Li, L.T. Canham, Electrochem. Solid-State Lett. 14 (2011) K25–K27.
[27] S.P. Low, N.H. Voelcker, L.T. Canham, K.A. Williams, Biomaterials 30 (2009) 2280–2873.
[28] J.C. Vial, J. Derrien, Porous Silicon Science and Technology, first ed., Springer, Berlin, 1995.
[29] O. Bisi, S. Ossicini, L. Pavesi, Surf. Sci. Rep. 38 (2000) 1–126.
[30] L. Canham, Properties of Porous Silicon, first ed., INSPEC, London, 1997.
[31] L. De Stefano, I. Rendina, L. Moretti, A.M. Rossi, A. Lamberti, P. Arcari, in: P. Siciliano (Ed.), Sensors for Environmental Control, World Scientific, Singapore, 2003, pp. 46–50.
[32] X. Chen, J Zhu, Q. Xi, W. Yang, Sens. Actuators B 161 (2012) 646–654.
[33] W. Si, W. Lei, Z. Han, Y. Zhang, Q. Hao, M. Xia, Sens. Actuators B 193 (2014) 823–829.
[34] J. Li, J. Liu, G. Tan, J. Jiang, S. Peng, M. Deng, D. Qian, Y. Feng, Y. Liu, Biosens. Bioelectron. 54 (2014) 468–475.
[35] B. Habibi, M. Abazari, M.H. Pournaghi-Azar, Colloid Surf. B 114 (2014) 89–95.
[36] Y.F. Li, K.J. Li, G. Song, J. Liu, K. Zhang, B.X. Ye, Sens. Actuators B 182 (2013) 401–407.
[37] M.H. Pournaghi-Azar, A. Saadatirad, Electroanalysis 22 (2010) 1592–1598.
[38] A. Afkhami, H. Khoshsafar, H. Bagheri, T. Madrakian, Sens. Actuators B 203 (2014) 909–918.
[39] A.A. Ensafi, M.M. Abarghoui, B. Rezaei, Sens. Actuators B 196 (2014) 398–405.
[40] J.M. Westra, V. Vavrunkova, P. Sutta, R.A.C.M.M. van Swaaij, M. Zeman, Energy Procedia 2 (2010) 235–241.
[41] F. Zhu, G. Ma, Z. Bai, R. Hang, B. Tang, Z. Zhang, X. Wang, J. Power Sources 242 (2013) 610–620.
[42] A. Safavi, M. Tohidi, Anal. Chem. 83 (2011) 5502–5510.